Article

Corrosion Electrochemical Behavior of 2024 Aluminum Alloy in Potassium Acetate Deicing Fluid

Lin Xiuzhou, [ID] *,a,b Zhao Wei,a Yang Feng,c Yang Han,a Peng Qiang,a Mei Yongjun,d Wang Yuhaoa and Dou Baojie [ID] *,a,b

aSchool of Materials Science and Engineering, Sichuan University of Science & Engineering, Zigong 643000, China

bMaterial Corrosion and Protection Key Laboratory of Sichuan Province, Sichuan University of Science & Engineering, Zigong 643000, China

cThe Thirtieth Research Institute of CETC, Chengdu 610093, P. R. China

dThe Second Research Institute of CAAC, Chengdu 610041, P. R. China

The low-temperature electrochemical corrosion behavior of aircraft 2024 aluminum alloy was investigated in different concentrations of potassium-acetate-type fluid, and the results showed that the corrosion medium initially impacted some corrosiveness on the 2024 aluminum alloy. However, the corrosion rate of the alloy decreased with prolonged immersion in the corrosion medium, and this was attributed to the protective effect of the corrosion products layer, which impeded the attack by the aggressive solution. Time-domain analysis of electrochemical noise measurements at −5 °C revealed the occurrence of uniform corrosion on the alloy at the initial stages of immersion, general corrosion at the middle stages of immersion, and a pitting-dominated corrosion type from the middle to late stages of immersion.

Keywords: aluminum alloy, deicing fluid, corrosion, low temperature, electrochemical impedance spectroscopy, electrochemical noise

Introduction

In an environment with harsh ice and snow, sediments such as ice, frost, and snow can seriously threaten aircraft safety.[1-3] At present, the most effective way to deal with aircraft icing/anti-icing is to use a deicing/anti-icing fluid. Deicing fluids are mainly divided into four types: types I, II, III, and IV. The standards stipulate that the freezing point depressants of type-I aircraft deicing fluids[4-6] can be alcohol-based and non-alcohol-based compounds. The chemical oxygen demand (COD) and biological oxygen demand (BOD) values of an alcohol-based deicing fluid are extremely high, and its waste fluid significantly affects the ecological environment around the airport.[7-10] The alkali-metal organic-acid salt-type deicing fluid used for runway deicing[11] has a low cost, a good anti-icing/deicing effect, and extremely low COD and BOD values, and it does not cause environmental pollution problems.

At present, the 2024 aluminum alloy is still mainly used for the fuselage skin, under-wing skin, long stringer, chord beam, and lower surfaces of the horizontal wings for most models.[12-14] The corrosion in these parts is found by the airline during the maintenance of the aircraft. The ASTM F1110[15] standard specifies the test standard of the effect of aviation chemicals on the corrosion of aircraft aluminum alloys. Many efforts have been focused on the corrosion behavior of chromium-plated steel for aircraft in full immersion in potassium acetate road surface de-icing solution;[16] Zhang *et al.*[17] studied the ice-sparing coating of aircraft cabin icing mitigation by potassium acetate road surface de-icing solution and proved that the potassium acetate-based de-icing solution greatly reduced the performance of the ice-sparing layer; this group has also studied the corrosion behavior of 4130 steel in the thin liquid film state of potassium acetate de-icing solution in the early stage of the project. There is little research focusing on ice protection and wettability change on Al alloy.[18] Besides, the corrosion properties of Al alloys in potassium acetate de-icing solution at 23, 80, and 120 °C

*e-mail: linxiuzhou@suse.edu.cn; baojiedou@suse.edu.cn

have been studied.[19] However, the corrosion of Al alloys in potassium acetate de-icing solution at low temperatures has not been comprehensively studied, so the standard is still not good enough to evaluate the corrosion effect of the de-icing solution on aircraft aluminum alloy during actual aircraft de-/anti-icing operations.

The electrochemical corrosion behavior of the 2024 aluminum alloy in a potassium-acetate-type deicing fluid at −5 °C was studied in this work. The results provide a theoretical basis and data support for understanding the corrosion behavior, and they offer guidance for the development and application of new aircraft deicing fluids.

Experimental

Materials

The specific composition of the 2024-T3 (solid solution and natural aging treatment) aluminum alloy used in the study is shown in Table 1, supplied by the MD Aluminum industry (Suzhou, China). The material was a 2024-T3 aluminum alloy bar with a diameter of 10 mm. The sample was sealed with epoxy resin (E-44) and polyamide curing agent (PA-651) which were purchased from Nantong Xingchen Synthetic Material Co., Ltd (Nantong, China). The samples were subsequently cured in a drying oven at 40 °C for 24 h. Then, the samples were ground and polished with SiC sandpaper and polishing paste, respectively. Finally, it was rinsed with alcohol and dried in cold air. The potassium-acetate-type deicing fluid (N-6) used in the experiment was provided by the Second Research Institute of the Civil Aviation Administration of China (Chengdu, China).

Corrosion test

An electrolyte was the deicing fluid, which was diluted to 10, 25, and 50% with deionized water. Then, dry and wet alternating cycles of standing for 4 h in −5 °C electrolyte and air, respectively, were performed as a corrosion test (denoted by "T"). The PGSTAT302N Autolab electrochemical workstation (Utrecht, Netherlands) was employed for electrochemical measurements. It performed potentiodynamic polarization tests and alternating current electrochemical impedance spectroscopy (EIS) tests. The electrochemical setup consisted of a three-electrode cell containing the 2024-T3 aluminum alloy as the working electrode, a platinum sheet as the counter electrode, and a saturated calomel electrode (SCE) as the reference electrode. Potentiodynamic polarization started from −0.3 V with reference to the open circuit potential to 1.0 V *vs*. E_{cor} at a rate of 1 mV s^{-1}. The EIS measurements were conducted at an alternating voltage with a 5 mV amplitude in the frequency range of 0.01-100 kHz at open circuit potential.[20,21] The EIS data was analyzed using the ZSimpWin software. Electrochemical noise (EN) was tested using a setup with a two-working-electrode cell containing two 2024-T3 aluminum alloys that were identical to the working electrode and a platinum sheet as the counter electrode. EN measurements were carried out at a sampling frequency of 4 Hz, and the tests were conducted for 1200 s. The electrochemical noise was measured using two working electrode systems, namely 2024 aluminum alloy WE_1 and WE_2, auxiliary electrode platinum electrode. The sampling interval was 0.25 s, sampling frequency was 4 Hz, sampling time was 1200 s, a total of 4800 data points.[22,23]

Corrosion morphology and product analysis

The morphology of corrosion products was observed by VEGA 2 SBU TESCAN scanning electron microscope (Brno, Czech Republic), and the contents of Al, O, Mg, Cu and other elements in the corrosion products on the surface of 2024 aluminum alloy were characterized by X-ray energy dispersive spectrometer (EDS). The accelerating voltages were 10 and 15 kV, respectively.

Results and Discussion

Polarization curves

Figure 1 shows the polarization curves for the 2024-T3 aluminum alloy samples in different concentrations of deicing fluid, and Table 2 shows the corrosion data after fitting. After the final corrosion cycle, the corrosion current was significantly lower than the initial value. This was due to the protective layer on the sample provided by the corrosion products that were generated on the aluminum alloy surface with the prolongation of the corrosion time.

The generation of the deicing fluid was also an important factor affecting the corrosion of the 2024-T3

Table 1. The main chemical composition of the 2024 aluminum alloy

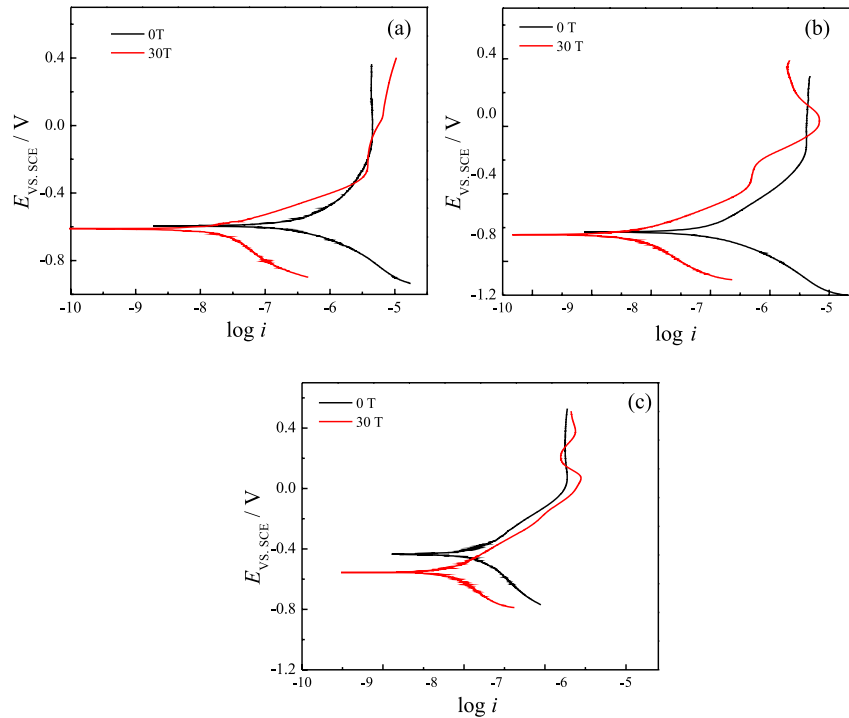| Composition	Cu	Si	Fe	Mn	Mg	Zn	Cr	Ti	Al
Content / %	4.33	0.33	0.19	0.61	1.57	0.14	0.04	0.06	balance

Figure 1. Polarization curves of 2024 aluminum alloy exposed to different concentrations (a) 10%, (b) 25%, (c) 50% of potassium acetate type deicing fluid at initial and 30 dry and wet alternating cycles (30 T).

aluminum alloy. According to Table 2, the corrosion current of the sample increased gradually as the amount of deicing fluid generation decreased. This showed that the corrosion inhibitor in the deicing fluid had an important protective effect on the aluminum alloy. In the deicing fluid, the corrosion inhibitor decreased with the decrease in the concentration of deicing fluid. As a result, the protection for the sample decreased and the corrosion rate increased.

Table 2. Fitting results of polarization curve for 2024 aluminum alloy exposed to potassium-acetate-type deicing at initial and 30 dry and wet alternating cycles (30 T)

Concentration / %	T	E_{cor} / V_{SCE}	i_{cor} / (A cm^{-2})
10	0	−0.586 ± 0.003	3.075×10^{-7} ± 0.501
	30	−0.611 ± 0.005	2.164×10^{-8} ± 0.431
25	0	−0.613 ± 0.018	1.556×10^{-7} ± 0.211
	30	−0.638 ± 0.025	1.180×10^{-8} ± 0.062
50	0	−0.430 ± 0.050	2.052×10^{-8} ± 0.352
	30	−0.553 ± 0.009	4.581×10^{-9} ± 0.468

T: dry and wet alternating cycles of standing for 4 h in −5 °C electrolyte and air, respectively; E_{cor}: self-corrosion potential; i_{cor}: self-corrosion current.

Electrochemical impedance spectroscopy

To evaluate the corrosion performance of 2024 aluminum alloy in different concentrations of potassium acetate de-icing solution, the EIS data of the aluminum alloy in 10, 25 and 50% potassium acetate de-icing solution were presented in Figure 2. Also, the fitted curves based on the corresponding equivalent circuits were shown. The fitted circuits used were shown in Figures 3a and 3b, where Figure 3a is for 0 T and Figure 3b for 1-30 T. R_s denoted the potassium acetate solution resistance, i.e., the resistance between the working electrode and the reference electrode, R_f and Q_f are the resistance and capacitance of the film formed by adsorption of corrosion products and corrosion inhibitor, respectively, Q_{dl} denoted the constant phase element of the double-layer capacitance, and R_{ct} was the charge transfer resistance. From Figure 2, it can be seen that there are two time constants appearing at 1-30 T for all the samples, which was attributed to the organosilicon-based adsorption type corrosion inhibitor contained in the potassium acetate type de-icing solution and the electrochemical corrosion reaction at the solution/substrate interface. As to the 10% concentration sample, the low-frequency impedance modulus shows a decrease-increase-decrease-increase as the corrosion cycle proceeds and reaches a minimum of 4.4×10^5 Ω cm^2 at 16 T, as shown in Figure 4a. This is because the corrosion inhibitor concentration is low, and the aluminum alloy substrate is in contact with the solution and rapidly generates a passivation film that retard the corrosion rate of the substrate. As to 25 and 50% concentration samples, the low-frequency impedance modulus shows a decrease and then increases change and reaches a minimum of 5.0×10^5 Ω cm^2 at 19 T

for 25% concentration sample, and reaches a minimum of $5.4 \times 10^5 \ \Omega \ cm^2$ at 22 T for 50% concentration sample, as shown in Figure 4a. During 30 T, the 50% concentration sample shows the highest resistance because the corrosion inhibitor plays an important role in delaying corrosion. These results indicated that the de-icing solution has an effective inhibition on the corrosion of the aluminum alloy substrate. However, the inhibitor concentration will decrease with the melting of ice resulting in a decrease in the inhibition effect.

In order to further analyse the EIS data, the EIS data were fitted using the ZSimpWin software, and the fitting results of each equivalent element were shown in Table 3.

As shown in Figure 4b, the membrane resistance gradually decreased with the prolongation of the corrosion cycle in the higher-concentration deicing fluid, which was similar to that in the lower-concentration fluid with a lower volatility. As to 10% concentration sample, faster corrosion of the sample surface occurred, which then decreased rapidly and gradually stabilized. The low-concentration
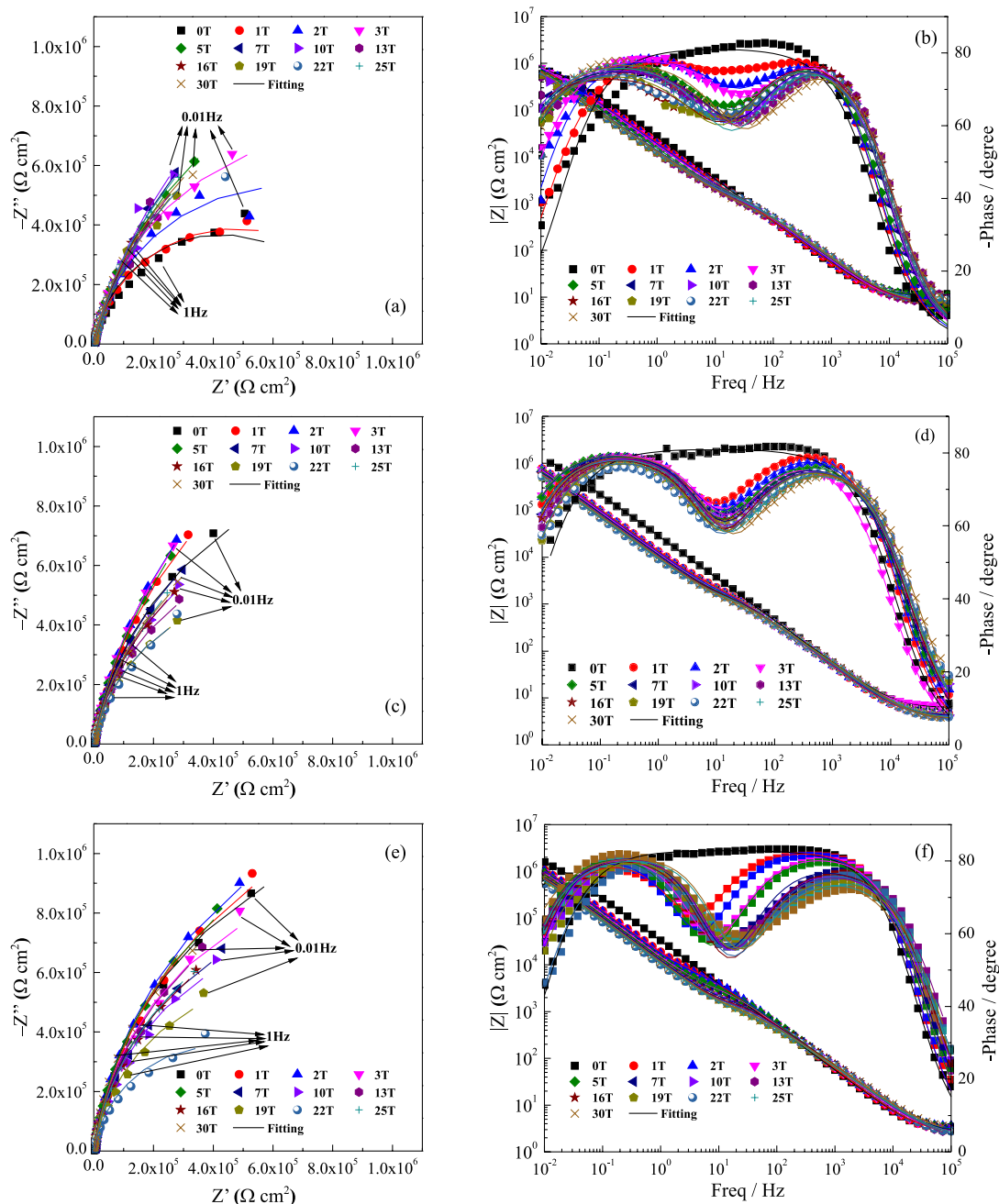

Figure 2. Electrochemical impedance spectroscopy (EIS) plots of 2024 aluminum alloy exposed to 10, 25, 50% potassium-acetate-type deicing fluid for different time periods: (a) 10% Nyquist plot, and (b) 10% Bode plot, (c) 25% Nyquist plot, and (d) 25% Bode plot, (e) 50% Nyquist plot, and (f) 50% Bode plot.
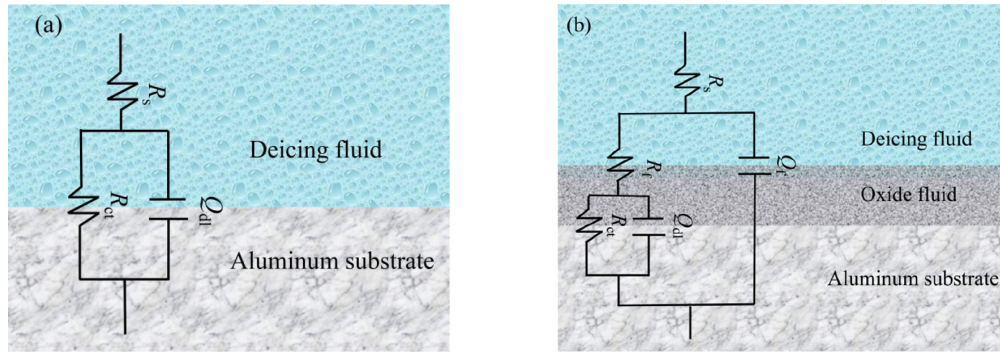
Figure 3. Fitting equivalent circuit model of electrochemical impedance spectroscopy (EIS).

Table 3. Equivalent circuit fitting results

Concentration / %	Fitting parameters	T												
		0	1	2	3	5	7	10	13	16	19	22	25	30
10		10.83	9.29	10.02	7.95	10.18	8.68	8.43	7.15	7.66	8.42	8.36	8.06	7.50
25	R_s / (Ω cm²)	6.12	4.19	4.16	6.48	3.94	3.93	3.68	3.40	3.73	3.46	3.23	3.65	3.07
50		2.87	2.70	3.03	2.56	2.77	2.58	2.30	1.75	2.26	1.90	2.01	2.13	2.49
10			5.87	5.67	5.38	5.48	5.39	5.53	5.39	5.80	6.22	6.14	5.78	5.70
25	Q_f / $\times 10^{-6}$ (F cm⁻²)		7.04	7.60	8.23	8.41	8.86	9.10	9.08	9.06	9.40	9.34	9.37	9.07
50			4.99	4.56	4.98	5.09	6.24	6.93	7.56	6.12	8.29	6.88	8.72	8.35
10			3.69	3.03	2.16	2.63	2.14	2.20	1.60	3.30	3.35	3.36	2.30	1.51
25	R_f / $\times 10^{3}$ (Ω cm²)		4.15	3.41	2.90	3.16	2.99	2.72	2.52	2.85	2.56	2.60	2.38	2.02
50			13.4	10.26	5.38	5.74	3.01	2.56	2.59	2.43	2.19	2.18	1.96	1.98
10		7.10	3.90	4.80	5.79	8.12	10.11	10.65	11.66	11.19	10.97	9.79	10.58	10.02
25	Q_{dl} / $\times 10^{-6}$ (F cm⁻²)	6.74	7.67	8.03	8.16	8.92	8.77	9.66	10.12	10.55	11.71	12.30	10.76	18.84
50		5.61	5.64	6.71	7.51	8.30	8.56	8.96	8.65	10.75	9.26	11.38	8.30	7.56
10		0.85	0.95	1.27	1.69	2.46	3.01	3.20	2.48	4.16	2.39	2.26	2.57	2.20
25	R_{ct} / $\times 10^{6}$ (Ω cm²)	2.15	2.85	3.25	3.15	2.97	2.16	1.78	1.48	1.83	1.18	1.18	2.01	1.88
50		2.42	2.60	2.66	2.01	2.45	1.77	1.63	2.12	1.81	1.31	0.81	2.01	2.95

T: dry and wet alternating cycles of standing for 4 h in −5 °C electrolyte and air, respectively; R_s: solution resistance; Q_f: membrane phase element; R_f: phase element resistance; Q_{dl}: charge transfer resistance phase element; R_{ct}: charge transfer resistance.

deicing fluid had a lower inhibitor concentration, which could not provide effective protection to the aluminum alloy, but the corrosion was hindered after the passivation film formed. In the high-concentration solution, the corrosion inhibitor could protect the 2024 aluminum alloy effectively; so, the corrosion rate was lower than that in the 10% solution. However, as the corrosion time increased, the performance of the corrosion inhibitor decreased, and the corrosion rate of the aluminum alloy increased. Moreover, with the formation and dissolution of the passivation film on the surface of the aluminum alloy, when the corrosion reached about 23 T, the three systems reached a dynamic balance, and the corrosion rate attained maximum values. As shown in Figure 4c, in the beginning, the charge transfer resistance of 25 and 50% concentration samples are higher than that of 10% concentration sample, because of the high concentration inhibitor adsorption on the surface of the aluminum substrate to increase the charge transfer resistance. Then, the performance of the corrosion inhibitor decreased with the increase of the corrosion time, and the charge transfer resistance decreased and reached a stable corrosion reaction.

Electrochemical noise

Time-domain analysis

Figure 5 shows the variation of EN with time for the 2024 aluminum alloy after third-order polynomial de-drift[22,23] in 10% potassium-acetate-type deicing solution. The potential noise intensity of the sample underwent a distinct process of first increasing and then decreasing with the prolongation of the corrosion time. During the initial corrosion, the potential noise of the sample had a high vibration frequency, and dense transient peaks appeared in the current noise 100 s
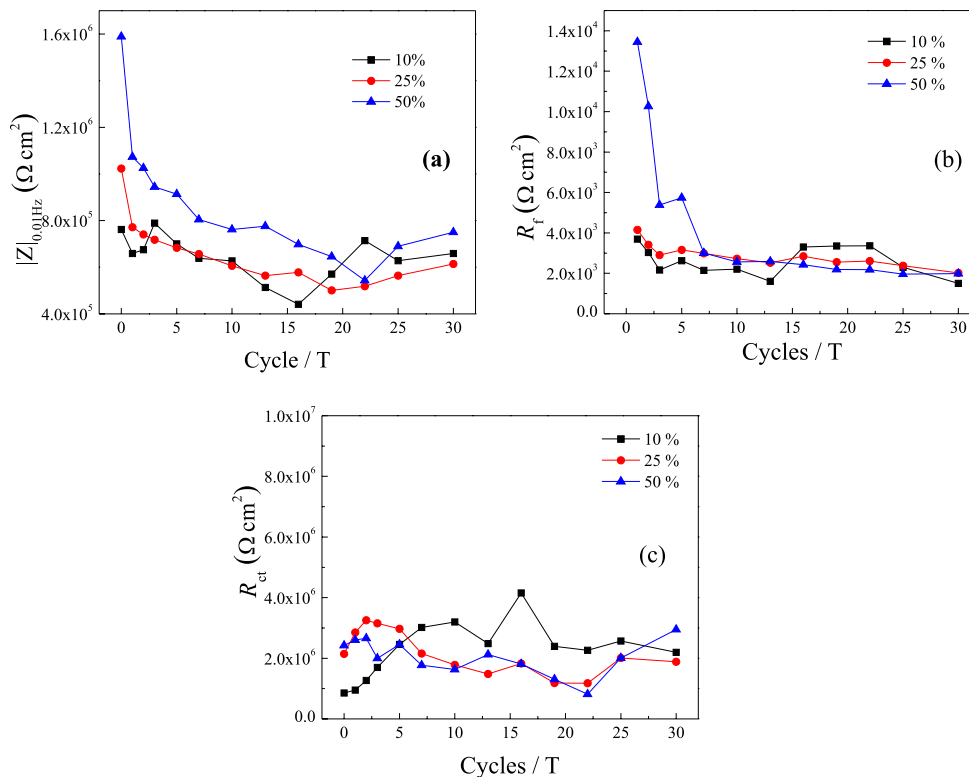
Figure 4. Electrochemical impedance spectroscopy (EIS) of 2024 aluminum alloy exposed to potassium-acetate-type deicing fluid for different time periods: (a) low-frequency modulus $|Z|_{0.01Hz}$ and fitting data (b) R_f, (c) R_{ct}.

before the test, which decreased significantly after 100 s, and no characteristic peaks appeared. The transient peaks were basically symmetric. At this time, the surface of the sample was mainly uniform corrosion. When the corrosion reached six cycles (6 T), in the first 500 s of the test, the vibration frequency of the potential noise of the sample was lower than that of the initial sample. After 500 s, the potential noise fluctuated at a higher frequency, and the sample was mainly corroded by general corrosion. Between 24 and 36 cycles (24-36 T), the vibration frequency of the potential noise increased, less significant transient peaks appeared, and the potential noise intensity gradually decreased. After 60 corrosion cycles (60 T), the potential noise intensity of the sample decreased, the vibration frequency increased, a transient peak appeared, and the 2024 aluminum alloy sample exhibited localized corrosion.

Frequency-domain analysis

The fast Fourier transform (FFT) was used for further processing to obtain the power spectral density (PSD) map of the 2024 aluminum alloy after corroding in a 10% deicing solution for different time periods. The results are shown in Figure 6.

The PSD was related to the frequency (*f*) as follows:

$$\log(PSD) = A + k\log f \tag{1}$$

where A is the noise intensity, and k is the slope of the high-frequency region of the PSD curve. The linear part of the high-frequency region of the PSD map was fitted to obtain the slope k of the high-frequency part of the noise PSD curve, as shown in Table 4.

W represents the white noise level. W and k can be used to analyze the corrosion tendency and corrosion strength of the working electrode surface,[24,25] the larger the W value of the voltage noise, the smaller the current noise W, and the lower the corrosion resistance of the material. The W_V (potential white noise level) value of the 2024 aluminum alloy generally increased first and then decreased. Therefore, the corrosion tendency of the sample increased first and then decreased, while the variation trend of W_I (current white noise level) was opposite to that of W_V, which first decreased and then increased. The corrosion tendency reflected by it was consistent with W_V.

The values of k_V (slope of the high frequency region of the power spectral density curve of the potential) changed from −2.02 (0 T) to −1.01 (6 T), and then changed to −2.09 (24 T), and then increased to −1.10 (60 T). The values of k_I (slope of the high frequency region of the power spectral density curve of the current) changed from −0.55 (0 T) to −0.45 (15 T), and then changed to −0.53 (24 T), and keep around −0.55 (60 T). Such change of k_V and k_I values indicated that the corrosion of 2024 aluminum alloy was
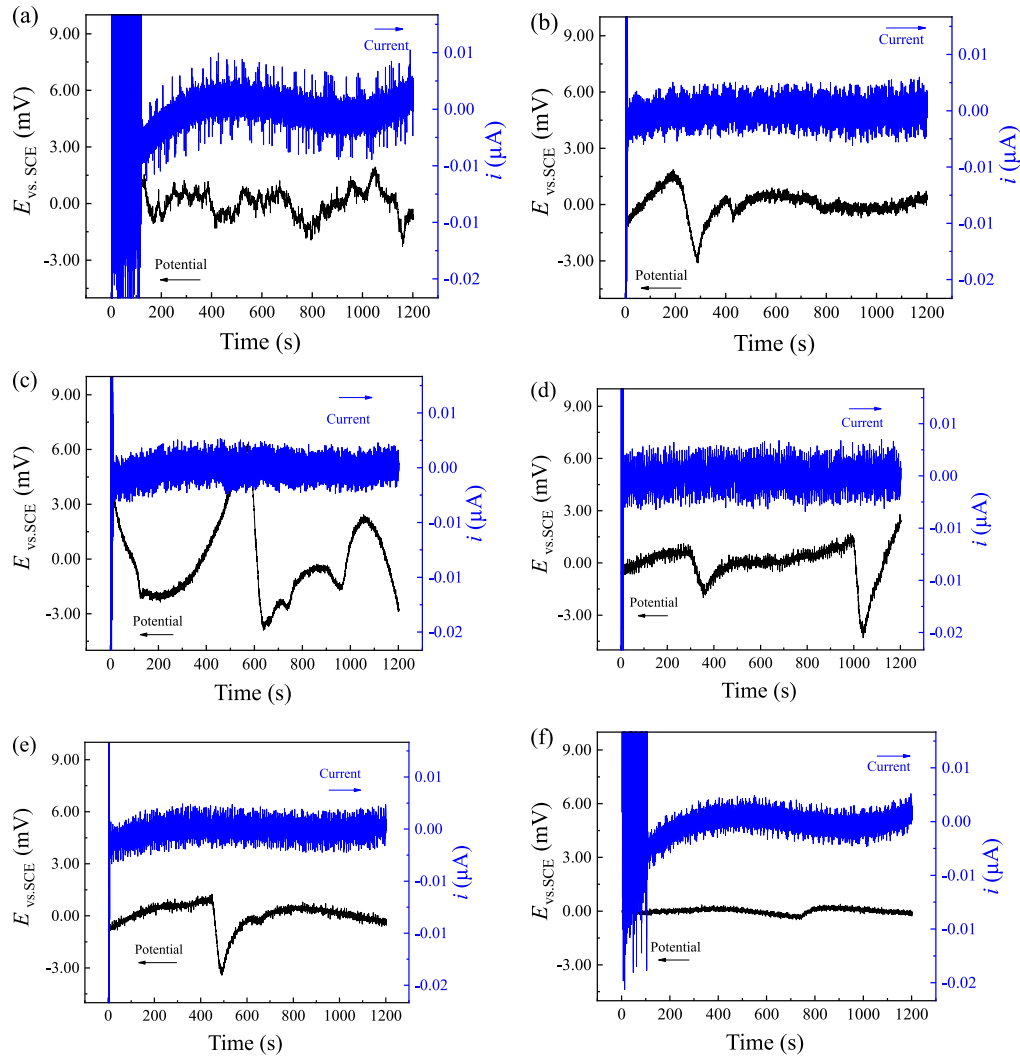
Figure 5. Electrochemical noise (EN) of 2024 aluminum alloy exposed to 10% potassium-acetate-type deicing fluid for different time periods: (a) 0 T, (b) 6 T, (c) 15 T, (d) 24 T, (e) 36 T, (f) 60 T.
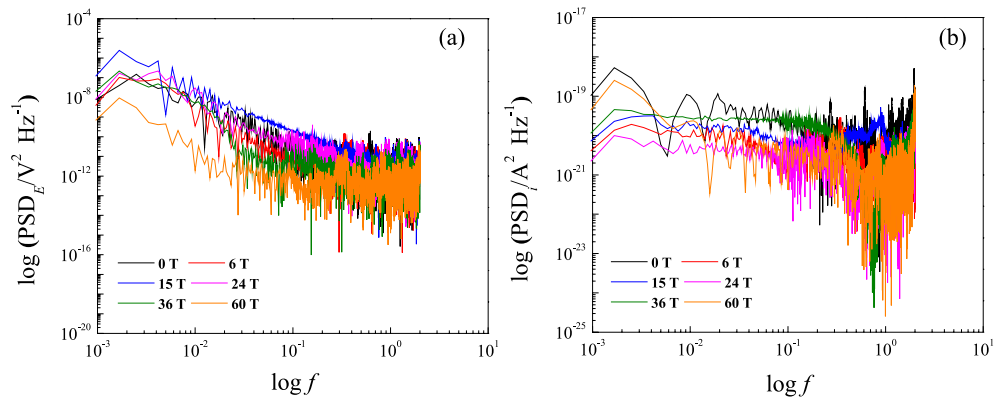

Figure 6. Power spectral density (PSD) curves of 2024 aluminum alloy exposed to 10% potassium-acetate-type deicing fluid: (a) potential PSD and (b) current PSD.

dominated by various corrosion mechanisms.[26,27] The first stage should be from 0 to 6 T, an oxide film gradually formed on the surface of 2024 aluminum alloy. The second stage is from 6 to 24 T, there should be some pitting

corrosion occurring on the local surface of 2024 aluminum alloy. At the last stage, the pitting corrosion increased, and the corrosion products accumulated on the surface of 2024 aluminum alloy.

Table 4. White noise and linear slope of 2024 aluminum alloy exposed to 10% potassium-acetate-type deicing for the different time periods

Cycle	W_V / (A² Hz⁻¹)	W_I / (A² Hz⁻¹)	k_V / (dB dec⁻¹)	k_I / (dB dec⁻¹)
0 T	−7.78	−19.08	−2.02	−0.55
6 T	−7.73	−19.96	−1.01	−0.50
15 T	−6.70	−19.75	−1.82	−0.45
24 T	−7.42	−20.31	−2.09	−0.53
36 T	−7.68	−19.56	−1.64	−0.52
60 T	−9.24	−19.48	−1.10	−0.55

W_V: potential white noise level; W_I: current white noise level; k_V: slope of the high frequency region of the power spectral density curve of the potential; k_I: slope of the high frequency region of the power spectral density curve of the current; T: dry and wet alternating cycles of standing for 4 h in −5 °C electrolyte and air, respectively.

Corrosion morphology

Figure 7 shows the surface morphology of the 2024 aluminum alloy after corrosion in the 50% deicing solution. After corrosion, distinct corrosion products formed on the surface of the sample, and the formed corrosion products were loose. In the vicinity of some of the corrosion products, grooves appeared in the substrate. In addition, a small and thin layer of corrosion product film formed near the corrosion products. Local elemental analysis showed that the corrosion products were mainly composed of C, O, Cu, Mg, Al, K, and other elements, of which K was mainly derived from the residue of the deicing liquid, C was mainly derived from the corrosion product Al(hac)₃ (hac is the abbreviation of CH_3COO), and Cu and Mg were derived from the second phase of the 2024 aluminum alloy. The peak intensities of O and Al were the highest, indicating that these two elements were the main elements of the corrosion products.

The pH of the potassium-acetate-type deicing solution was between 9.3 and 9.6 when the concentration was 10-50%. Therefore, the corrosion of the 2024 aluminum alloy
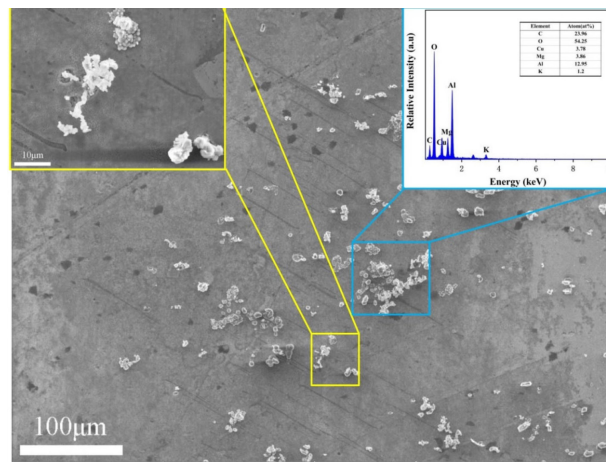

Figure 7. Surface morphology and energy spectrum analysis of corrosion products of 2024 aluminum alloy exposed to 50% potassium acetate type deicing solution for 30 T.

in the potassium-acetate-deicing solution occurred in an alkaline environment, and its electrochemical reactions were as follows:

$$Al + 4OH^- = Al(OH)_4^- + 3e^- \qquad (2)$$
$$2H_2O + 2e^- = 2OH^- + H_2 \qquad (3)$$
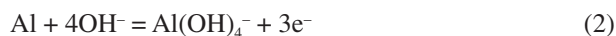
The corrosion of aluminum in an alkaline environment is usually accompanied by a hydrogen evolution process,[28,29] and the hydrogen evolution reaction occurs between the surface of the aluminum substrate and the adsorption layer of the corrosion products, which has a certain destructive effect on the formed corrosion product film.

Figure 8 shows the corrosion mechanism of 2024-T3 aluminum alloy in potassium acetate deicing solution. The oxide film on the surface of the aluminum alloy was dissolved in the potassium-acetate-type deicing liquid, and the matrix formed holes and active points. At each active site, the three electrons of the aluminum atom were successively lost, forming a corrosion product composed
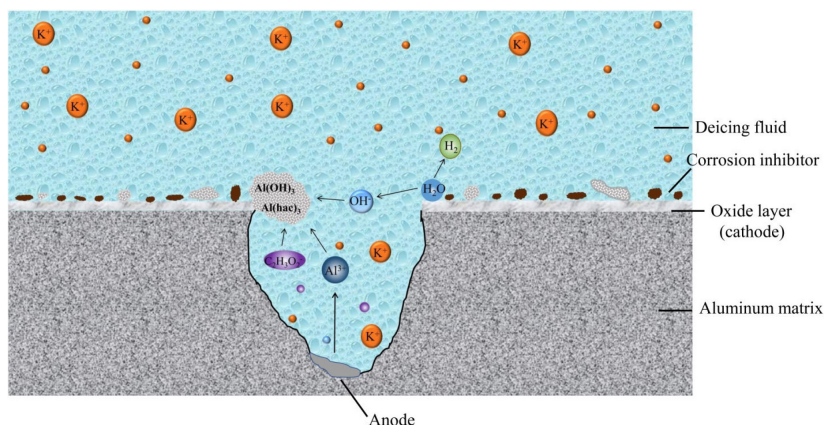
Figure 8. Corrosion mechanism of 2024 aluminum alloy in potassium acetate deicing fluid.

of Al(OH)$_3$ and Al(hac)$_3$ with hydroxide and acetate in the solution, which adhered to the substrate surface to slow the further corrosion, while the hydrogen ions of the water molecules combined with the electrons to generate H$_2$ and precipitate out. The potassium acetate deicing solution contains adsorption corrosion inhibitor, which can alleviate the corrosion of aluminum alloy in the solution.

Conclusions

In low-concentration deicing fluid, the concentration of the corrosion inhibitor was very low, and the fluid did not function. The corrosion rate of the aluminum alloy was mainly affected by the formation and evolution of the corrosion product film. In the early stage of corrosion, the corrosion rate of the 2024 aluminum alloy was relatively large, and then, the corrosion rate decreased rapidly and gradually became stable due to the passive film formed on the surface hindering the corrosion. In addition, in the deicing solution with a higher concentration, the corrosion inhibitor had a significant protective effect. With the formation and dissolution of the passivation film on the surface of the aluminum alloy, the variation process of the corrosion rate was more complicated. In the early stage of corrosion, the effect of the corrosion inhibitor was dominant, and the corrosion rate of the aluminum alloy was lower than that of the low-concentration deicing fluid. As the corrosion time increased, the performance of the corrosion inhibitor decreased, and the corrosion rate gradually increased. Subsequently, the passive film continued to form and dominate, and the corrosion rate of the aluminum alloy decreased again at the end of the corrosion. In the early stage of corrosion, the electrochemical noise of the 2024 aluminum alloy had a symmetric transient peak, which showed uniform corrosion. In the middle stage of corrosion, the transient peak was asymmetric, showing general corrosion. In the middle and late stages of corrosion, the transient peak-to-peak value increased, and a large number of transient peaks of high-frequency vibrations appeared, which manifested as pitting corrosion.

Acknowledgments

Author Contributions

Lin Xiuzhou was responsible for formal analysis funding acquisition; Zhao Wei for writing original draft; Yang Feng for validation; Yang Han for investigation; Peng Qiang for writing-review and editing; Mei Yongjun for resources; Wang Yuhao for writing-review and editing; Dou Baojie for project administration.

References

1. Ignatyev, D. I.; Khrabrov, A. N.; Kortukova, A. I.; Alieva, D. A.; Sidoryuk, M. E.; Bazhenov, S. G.; *Aerosp. Sci. Technol.* **2020**, *104*, 105914. [Crossref]

2. Huang, X.; Tepylo, N.; Pommier-Budinger, V.; Budinger, M.; Bonaccurso, E.; Villedieu, P.; Bennani, L.; *Prog. Aeronaut. Sci.* **2019**, *105*, 74. [Crossref]

3. Gent, R. W.; Dart, N. P.; Cansdale, J. T.; *Philos. Trans. R. Soc., A* **2000**, *358*, 2873. [Crossref]

4. SAE AMS 1424: *Deicing/Anti-icing Fluid, Aircraft, SAE Type I*, SAE International: New York, USA, 2015. [Link] accessed in January 2023

5. ISO 11075: *Aircraft Deicing/Anti-icing Fluids- ISO Type I*, International Standards Organization: Genève, Switzerland, 2007. [Link] accessed in January 2023

6. GB/T 20856: *Aircraft Newton Type Deicing Anti-icing Fluid Type I*, Civil Aviation Administration of China: Beijing, 2012. [Link] accessed in January 2023

7. Schulz, M.; Comerton, L. J.; *J. - Water Pollut. Control Fed.* **1974**, *1*, 173. [Crossref]

8. Lin, X. Z.; Zhang, R. H.; Mei, Y. J.; Yang, L.; Yang, F.; Dou, B. J.; Wei, Y. Q.; *New J. Chem*. **2019**, *43*, 14435. [Crossref]

9. Zitomer, D. H.; Tonuk, G. U.; *J. Environ. Eng.* **2003**, *129*, 123. [Crossref]

10. Corsi, S. R.; Hall, D. W.; Geis, S. W.; *Environ. Toxicol. Chem.* **2001**, *20*, 1483. [Crossref]

11. Corsi, S. R.; Geis, S. W.; Bowman, G.; Failey, G. G.; Rutter, T. D.; *Environ. Sci. Technol*. **2009**, *43*, 40. [Crossref]

12. Nakai, M.; Eto, T.; *Mater. Sci. Eng., A* **2000**, *285*, 62. [Crossref]

13. Heinz, A.; Haszler, A.; Keidel, C.; Moldenhauer, S.; Benedictus, R.; Miller, W. S.; *Mater. Sci. Eng., A* **2000**, *280*, 102. [Crossref]

14. Bucci, R. J.; Warren, C. J.; Starke Jr., E. A.; *J. Aircraft* **2000**, *37*, 122. [Crossref]

15. ASTM F1110: *Standard Test Method for Sandwich Corrosion Test*, ASTM International: West Conshohocken (PA), 2014. [Link] accessed in January 2023

16. Zhang, Y. B.; Peng, H. Q.; Su, Z. L.; Wang, Q.; Lin, X. Z.; *Corros. Prot.* **2016**, *37*, 868. [Crossref]

17. Zhang, Z. C.; A, L.; Hu, H. Y.; Bai, X. L.; Hu, H.; *Aerosp. Sci. Technol.* **2021**, *119*, 107090. [Crossref]

18. Grishaev, V. G.; Borodulin, I. S.; Usachev, I. A.; Amirfazli, A.; Drachev, V. P.; Rudenko, N. I.; Gattarov, R. K.; Bakulin, I.

K.; Makarov, M. V.; Akhatov, I. S.; *Int. Commun. Heat Mass. Transfer* **2021**, *129*, 105698 [Crossref]

19. Rippy, K. C.; Volk, E.; Beers, R.; Kozubal, E.; Gauderman, K.; Vidal, J.; *Energies* **2022**, *15*, 4421. [Crossref]

20. Wang, L. W.; Liang, J. M.; Li, H.; Cheng, L. J.; Cui, Z. Y.; *Corros. Sci.* **2021**, *178*, 109076. [Crossref]

21. Ge, F.; Lin, F.; Liang, J. M.; Pang, K.; Li, H.; Wang, X.; Cui, Z. Y.; *Acta Metall. Sin.* **2021**, *34*, 1679. [Crossref]

22. Huang, J. Y.; Qiu, Y. B.; Guo, X. P.; *Corros. Eng., Sci. Technol.* **2010**, *45*, 288. [Crossref]

23. Hu, J. Y.; Wang, S. Y.; Lu, Y. Y.; Li, S.; *Constr. Build. Mater.* **2021**, *313*, 125474. [Crossref]

24. Cui, J.; Yu, D. Y.; Long, Z. W.; Xi, B. D.; He, X. S.; Pei, Y. S.; *J. Electroanal. Chem.* **2019**, *855*, 113584. [Crossref]

25. Zhang, Z.; Yuan, X. L.; Zhao, Z. Y.; Li, X. F.; Liu, B.; Bai, P. K.; *J. Electroanal. Chem.* **2021**, *894*, 115351. [Crossref]

26. Zhang, T.; Shao, Y. W.; Meng, G. Z.; Wang, F. H.; *Electrochim. Acta* **2007**, *53*, 561. [Crossref]

27. Zhang, T.; Liu, X. L.; Shao, Y. W.; Meng, G. Z.; Wang, F. H.; *Corros. Sci.* **2008**, *50*, 3500. [Crossref]

28. Armstrong, R. D.; Braham, V. J.; *Corros. Sci.* **1996**, *38*, 1463. [Crossref]

29. Bernard, J.; Chatenet, M.; Dalard, F.; *Electrochim. Acta* **2006**, *52*, 86. [Crossref]